Industrial Chemistry & Materials

Online ISSN 2755-2500
Print ISSN 2755-2608
Volume 2 Number 3
August 2024
rsc.li/icm

Themed issue
Liquid-based Materials: Novel Concepts from Fundamentals to Applications

COMMUNICATION
Shaojie Wang, Xu Hou *et al.*
Electrostatically responsive liquid gating system for controlled microbubble generation

ROYAL SOCIETY OF CHEMISTRY

ICM
Industrial Chemistry & Materials

Industrial Chemistry & Materials

ROYAL SOCIETY OF CHEMISTRY

COMMUNICATION

View Article Online
View Journal | View Issue

Cite this: *Ind. Chem. Mater.*, 2024, **2**, 424

Received 5th April 2024,
Accepted 4th June 2024

DOI: 10.1039/d4im00037d

rsc.li/icm

Electrostatically responsive liquid gating system for controlled microbubble generation†

Guochao Zeng,‡[a] Yunmao Zhang,‡[b] Zhongyi Fang,[a] Lejian Yu,[a] Yawen Zhang,[a] Shaojie Wang*[c] and Xu Hou *[abd]

Microbubbles have attracted considerable attention due to their distinctive properties, such as large surface area, inherent self-compression, and exceptional mass transfer efficiency. These features render microbubbles valuable across a diverse range of industries, such as water treatment, mineral flotation, and the food industry. While several methods for microbubble generation exist, the gas–liquid membrane dispersion technique emerges as a reproducible and efficient alternative. Nevertheless, conventional approaches struggle to achieve active *in situ* control of bubble generation. In this study, we introduce an electrostatically responsive liquid gating system (ERLGS) designed for the active management of microbubble production. Utilizing electric fields and anionic surfactants, our system showcases the capability to dynamically regulate bubble size by manipulating the solid–liquid adsorption. Experiments confirm that this active control relies on the electrostatic adsorption and desorption of anionic surfactants, thereby regulating the interactions among the solid–liquid–gas interfaces. Our research elucidates the ERLGS's ability of precisely controlling the generation of bubbles *in situ*, enabling nearly one-order-of-magnitude change in bubble size, underscoring its applicability in various fields.

Keywords: Liquid gating system; Electrostatic response; Anionic surfactants; Adsorption and desorption; Microbubbles.

1 Introduction

Microbubbles have recently garnered significant attention due to their numerous advantages, including large surface area, inherent self-compression, negatively charged and hydrophobic surface, along with superior mass transfer capabilities.[1–3] These characteristics have led to their widespread utilization in numerous fields, including water treatment,[4] mineral flotation,[5] the food industry,[6] and pharmaceuticals.[7] For example, within the realm of water treatment, the diminutive size and extensive surface area of microbubbles contribute to enhanced gas–liquid mass transfer rates, thereby elevating the efficiency of treatment processes.[8] Likewise, in the field of mineral flotation, microbubbles demonstrate a remarkable efficiency in recovering fine and ultrafine particles, thus improving the yield of particle recovery.[9] Due to the significant impact of size on properties such as surface area and mass transfer behaviour of microbubbles, controlling their size is crucial for their applications.[10–13]

Several methods for microbubble generation have been reported, including electrolysis,[14] dissolved air flotation,[15] ultrasonic methods,[16] venturi microbubble generators,[17] and microfluidics.[18] Nevertheless, these methods frequently suffer from limitations in efficiency, simplicity or controllability. In contrast, gas–liquid membrane dispersion technique presents a reproducible, controllable, energy-efficient, and readily scalable solution.[19] This method involves pressurizing gas through a microporous membrane to produce microbubbles, with the membrane's pore size and surface wettability significantly affecting the resultant microbubble sizes, which, in turn, have a pivotal impact on bubble properties.[20–22] However, the active *in situ* control of bubble sizes appears nearly unachievable, attributable to the static nature of the membrane's wettability and pore dimensions.[23,24]

Recently, liquid gating technology has been developed, involving the infusion of capillary-stabilized liquid into a porous substrate to create a dynamic and reconfigurable gate

[a] *State Key Laboratory of Physical Chemistry of Solid Surfaces, College of Chemistry and Chemical Engineering, Xiamen University, Xiamen 361005, China. E-mail: houx@xmu.edu.cn*
[b] *Department of Physics, Research Institute for Biomimetics and Soft Matter, Fujian Provincial Key Laboratory for Soft Functional Materials Research, Jiujiang Research Institute, College of Physical Science and Technology, Xiamen University, Xiamen 361005, China*
[c] *Department of Joint Surgery and Sports Medicine, Zhongshan Hospital, Xiamen University, Xiamen 361004, China. E-mail: wangshaojie@xmu.edu.cn*
[d] *Innovation Laboratory for Sciences and Technologies of Energy Materials of Fujian Province (IKKEM), Xiamen 361102, China*

† Electronic supplementary information (ESI) available. See DOI: https://doi.org/10.1039/d4im00037d

‡ Equally contributing authors.

for regulating fluid transport.[25,26] In such systems, the gating liquid fills and seals the micropores, requiring the transport fluid to deform the interface for pore entry.[27] Building on this foundation, various stimuli-responsive liquid gating systems have been conceptualized.[28] These systems are capable of activation by external stimuli including light,[29,30] magnetism,[31,32] temperature,[33] and acoustic fields,[34] finding successful applications in a wide range of fields such as multiphase separation,[35,36] chemical detection,[37,38] air purification,[13] and efficient emulsification.[39] Notably, the electrically responsive systems stand out due to their ease of operation, precise controllability, and rapid response, showcasing significant promise for the development of intelligent and responsive liquid gating systems.[40]

Here we introduce an electrostatically responsive liquid gating system (ERLGS) designed to facilitate active *in situ* control of microbubble generation. Utilizing electric fields combined with anionic surfactants, our methodology directly modulates the solid–liquid adsorption. This innovative approach allows for active regulation of the interactions among the solid–liquid–gas interfaces, which in turn influences the dynamics of bubble formation and detachment, thereby effectively altering the size of the bubbles produced, allowing for nearly one-order-of-magnitude change in bubble size with the use of small electric potentials, which holds significant implications for a wide range of practical applications. Compared with electrostatic spraying method which forms small bubbles by using strong non-uniform electric field, ERLGS has the benefit of not requiring large electric potentials (~2 V compared with ~10^3 V) and allowing the use of conductive liquid as opposed to insulating liquid media.[41–44]

2 Results and discussion

The electrostatically responsive liquid gating system (ERLGS) comprises a microporous membrane and a functional liquid. Specifically, the system utilizes a microporous stainless-steel membrane that is coated with gold (Fig. S1†), and the aqueous solution of sodium dodecyl sulfate (SDS), a negatively charged surfactant, serves as the functional liquid. When gas is pressurized through the system, microbubbles are generated during the membrane dispersion process. The ERLGS demonstrates the capability to alter the size of generated bubbles by nearly one order of magnitude (Fig. 1a). This significant alteration is facilitated through the electrostatic adsorption and desorption of anionic surfactants, achieved by applying small electric potentials.

The adsorption of anionic surfactant is closely correlated with the presence of surface charges at the solid–liquid interface.[45] The type and density of surface charges can be inferred from the sign and value of the difference between the open circuit potential (E_{OCP}) and the potential of zero charge (E_{PZC}). To access this, electrochemical impedance spectroscopy measurements were conducted in 1 mmol L^{-1} $NaClO_4$ solution to determine the differential capacitance (Fig. 2a). The observed minimum value, approximately 0.20 V, corresponds to the E_{PZC}. Meanwhile, the E_{OCP} value,

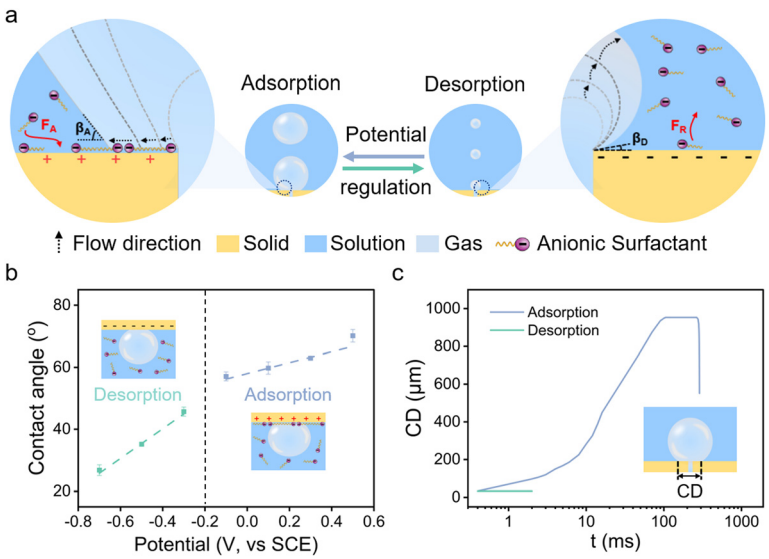

Fig. 1 Electrostatically responsive liquid gating system (ERLGS). (a) Schematic of the ERLGS for controlled bubble generation. The ERLGS consists of a microporous membrane and a function liquid containing negatively charged surfactant SDS. A positive potential attracts DS^- to adsorb on the membrane surface as a hydrophobic 'coating', leading to the formation of large bubbles during membrane dispersion process. A more negative potential electrostatically repels the negatively charged DS^- away from the surface, resulting in microbubbles; (b) contact angles of Au-coated stainless-steel sheet (Au/SSS) in 1 mmol L^{-1} SDS aqueous solution measured by captive bubble method at different electrode potentials; (c) the contact base diameters (CD) during bubble formation in 1 mmol L^{-1} SDS solution. In the desorption state, the bubble contact base aligns with the orifice size throughout bubble formation; whereas in the adsorption state, the bubble contact base extends to the membrane surface and is significantly greater than the orifice size.

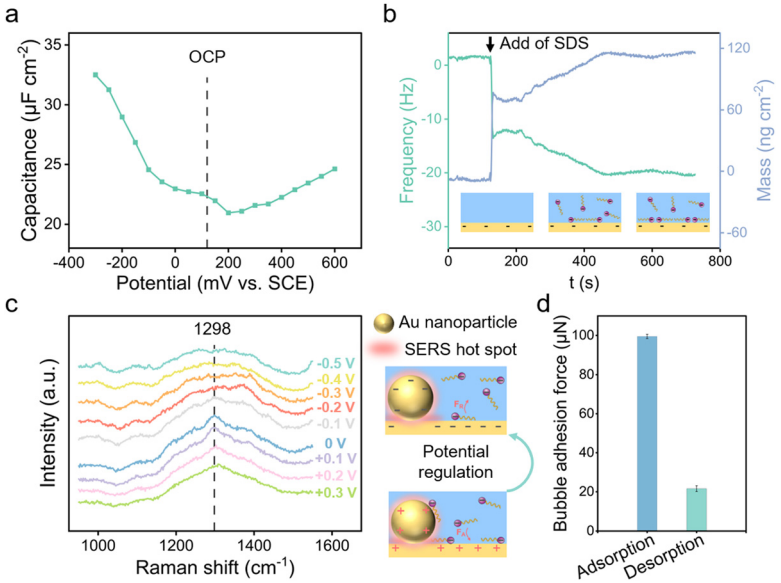

Fig. 2 Adsorption and desorption of anionic surfactants on the Au surface. (a) Differential capacitance of the Au surface in 1 mmol L^{-1} $NaClO_4$ solution. The minimum value, approximately 0.20 V, corresponds to the potential of zero charge (E_{PZC}). Meanwhile, the open circuit potential (E_{OCP}) value of about 0.12 V is negative than the E_{PZC} value, indicating a negatively charged surface under open circuit conditions; (b) change in frequency of Au-coated quartz crystal sensor upon adsorption of DS^- on the surface in 1 mmol L^{-1} SDS solution; (c) SERS spectra of the Au nanoparticle-coated Au electrode at different electrode potentials. The peak at 1298 cm^{-1} (originating from the dodecyl tail of DS^-) disappeared when the potential was negative than −0.2 V, indicating the desorption of DS^- from the surface due to electrostatic repulsion; (d) the bubble adhesion force of surface in the adsorption and desorption states.

measured at about 0.12 V, is negative than the E_{PZC} value, indicating the surface is negatively charged under open circuit conditions, which is further supported by the negative zeta potential of the surface (Fig. S2†).

The adsorption of DS^- on the surface was measured utilizing a quartz crystal microbalance (QCM). Following the introduction of the SDS solution, DS^- spontaneously adsorbed onto the surface, driven primarily by the dispersion force between the alkyl tail and the substrate,[46] causing a decrease in resonance frequency of quartz crystal sensor (Fig. 2b). For comparison, we measured the adsorption behaviour of SDS on the cysteamine-modified, positively charged Au surface. And it's demonstrated that more anionic surfactants DS^- adsorbed onto the positively charged surface than on the negatively charged Au surface (Fig. S3†).

To elucidate the mechanisms of electrostatic adsorption and desorption of dodecyl sulfate ions on the surface, electrochemical surface-enhanced Raman spectroscopy (EC-SERS) measurements were performed. Potentials were scanned from +0.3 V to −0.5 V with an interval of 0.1 V, revealing a 1298 cm^{-1} SERS peak originating from the alkyl chain of SDS at positive potentials (Fig. 2c and S4†).[47] This peak vanished when the potential was negative than −0.2 V, indicating the desorption of DS^- from the surface due to electrostatic repulsion.[48] Consequently, it is demonstrated that by varying the applied voltage, one can manipulate the adsorption and desorption of DS^- ions on the surface, thereby altering the surface's adherence to bubbles (Fig. 2d).

The wettability of membrane surface plays a key role in determining the pattern of bubble growth within the membrane dispersion process, thereby affecting the size of the generated bubbles (Fig. 1a). The employment of a positive potential induces the adsorption of DS^- ions onto the membrane surface as a hydrophobic 'coating', resulting in a large contact angle (Fig. 1b). Then the expansion force of a growing bubble exceeds the force for bubble closing, and the bubble develops by establishing a contact base on the membrane surface which is significantly greater than the size of the pore due to the nonwetting nature of the surface, leading to the generation of large bubbles (Fig. 1c and 3a). And the size of bubble becomes independent of the pore size. In contrast, a more negative potential electrostatically repels the negatively charged DS^- away from the surface, leading to a small contact angle (Fig. 1b). In this case, the expansion force is small and no contact base expansion is observed. That is, bubble growth is initiated at the pore edge, with the bubble contact base aligning with the pore size throughout bubble formation (Fig. 1c and 3b), resulting in the generation

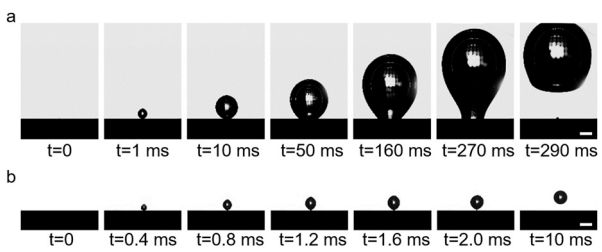

Fig. 3 Processes of bubble formation in the (a) adsorption state and (b) desorption state in 1 mmol L^{-1} SDS solution. Scale, 500 μm.

of microbubbles. And the size of the pore becomes the determining factor of the size of microbubbles. Therefore, by varying electric potentials, a reversible alteration in the membrane surface's wettability is achieved (Fig. S5†), which, in turn, modulates the size of the bubbles produce.

We further explored the impact of pore size and SDS concentration on bubble size (Fig. 4). It was observed that in the desorption state, the sizes of microbubbles escalate with an increase in pore size, while no similar trend is discernible in the adsorption state (Fig. 4a). This phenomenon aligns with prior conclusions and is attributed to the different patterns of bubble formation across these states. In the desorption state, the size of microbubbles (produced at the edge of the orifice) may be theoretically approximated by equating the buoyance force (F_b) with the surface tension force (F_s) acting upon the emerging bubble,[49] where

$$F_b = \frac{\pi}{6}\rho g {D_b}^3 \quad (1)$$

and

$$F_s = \pi D_p \gamma \sin\beta \quad (2)$$

Here, D_b and D_p represent the diameters of the bubble and pore, respectively, γ is the surface tension, ρ is the liquid density, and β is the dynamic contact angle observed during bubble growth. Assuming these two forces balance at the moment of a microbubble detaches from the orifice, the microbubble's diameter can be estimated as follows:

$$D_b = \left(\frac{6\gamma D_p \sin\beta}{\rho g}\right)^{\frac{1}{3}} \quad (3)$$

This equation effectively predicts the dependency of microbubble size on pore diameter (Fig. 4b). Notably, when a less negative potential was applied, the contact angle reduced slightly compared to that in the adsorption state, owing to the electrowetting effect (Fig. 1b).[50] Consequently, the size of the bubbles generated under this condition (denoted as 'weak adsorption state') lies intermediate to those observed in the adsorption and desorption states (Fig. 4a). Furthermore, owing to the rapid electrostatic adsorption and desorption of anionic surfactants, the ERLGS can achieve real-time (on the scale of seconds) modulation of the size of generated bubbles through the regulation of electric potentials (ESI† Movie).

In this ERLGS, the force required for the gas to overcome the capillary pressure at the interface is termed the transmembrane pressure, which can be well explained by the Laplace equation as follows:[51]

$$\Delta P = \frac{4\gamma\cos\theta}{D_p} + P_l \quad (4)$$

Here θ represents the contact angle and P_l is the hydrostatic pressure of the SDS solution. This equation effectively forecasts ΔP necessary for gas to traverse the ERLGS across varying pore sizes and states (Fig. 4c). The pressure differences in different states indicate that the ERLGS can achieve gas transport control under constant pressure, realizing an electrostatically responsive gating switch. Although smaller bubbles present a larger surface area relative to their gas volume, they necessitate a higher energy input due to an increased transmembrane pressure.

Upon the formation of a bubble in a surfactant solution, surfactant molecules will swiftly diffuse from the bulk solution

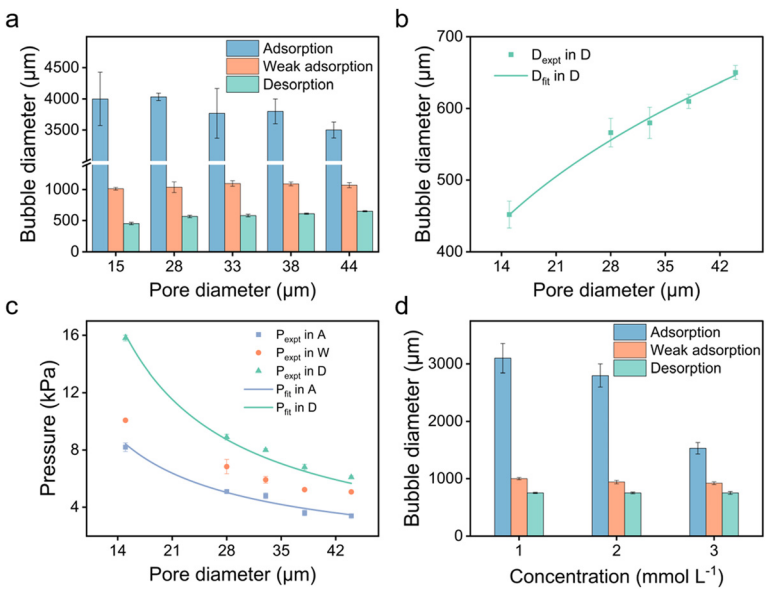

Fig. 4 Controlled bubble generation of ERLGS. (a) Diameters of bubbles generated from the ERLGS in 1 mmol L^{-1} SDS solution with different pore sizes in different states; (b) experimental and fitted value of bubble diameters generated with different pore sizes in the desorption state in 1 mmol L^{-1} SDS solution; (c) experimental and fitted value of transmembrane pressure for air passing through ERLGS with different pore sizes in different states in 1 mmol L^{-1} SDS solution; (d) diameters of bubbles generated with different SDS concentrations in different states.

to the bubble interface and reduce the surface tension (Fig. S6†). For SDS solution with a completely dissociated surfactant of the 1 : 1 electrolyte type, the quantity of surfactants adsorbed and surface tension is described by the following Gibbs adsorption equation:[52]

$$d\gamma = -2RT\Gamma d\ln C \quad (5)$$

where γ is the surface tension, R is the gas constant, T is the absolute temperature, Γ is the surface excess concentration and C is the molar concentration. Therefore, the more the quantity of surfactants adsorbed, the lower the surface tension. Experiments revealed that in the desorption state, the size of microbubbles remained relatively constant across different concentrations (Fig. 4d). This phenomenon can be attributed to the short duration of bubble growth in the desorption state (approximately 2 milliseconds, as shown in Fig. 1c), during which there is insufficient time for surfactants to adsorb onto the interface and effectively reduce the surface tension. In contrast, the duration of bubble growth in the adsorption state is significantly longer than in the desorption state (Fig. 1c), providing surfactants ample time to adsorb at the interface and lower the surface tension, which cannot effectively counteract buoyancy force and delay the detachment of growing bubble from the surface. Consequently, the size of large bubbles decreases with an increase in surfactant concentration (Fig. 4d).

To further demonstrate the use of anionic surfactants, comparative tests were conducted with two controls: sodium bromide (NaBr), a non-surfactant salt, and *N*-decanoyl-*N*-methylglucamine (MEGA-10), a nonionic surfactant. Although MEGA-10 is amphiphilic, its solution demonstrates notably poor electrical conductivity (Fig. 5a), leading to negligible variations in bubble size and transmembrane pressure across different potentials (Fig. 5c and d), indicative of no electric response. On the other hand, the NaBr solution exhibits good conductivity (Fig. 5a), facilitating modifications in wettability across varying potentials owing to the electrowetting effect (Fig. 5b). Nonetheless, the scope of modulation is significantly limited compared to that achieved with the SDS solution (Fig. 5b), where amphiphilic DS^- can adsorb onto the surface, forming a hydrophobic 'coating', enabling a wide range of adjustments in bubble size and transmembrane pressure (Fig. 5c and d). Therefore, it is the synergy of conductivity and amphiphilicity that grants the extensive tunability observed in SDS solution.

3 Conclusions

Our research presents an innovative electrostatically responsive liquid gating system (ERLGS) for precisely *in situ* controlling microbubble generation using anionic surfactants with the application of electric potentials. This method enables significant adjustments in bubble size, facilitating nearly one-order-of-magnitude change with minimal electric potential, which rely on the electrostatic adsorption and desorption of anionic surfactants, thereby regulating the interactions among the solid–liquid–gas interfaces. The study further explores the impact of pore size and SDS concentration on bubble size and highlights the importance of integrating conductivity and amphiphilicity to achieve extensive regulability in bubble generation, thereby laying the groundwork for sophisticated applications across a variety of disciplines.

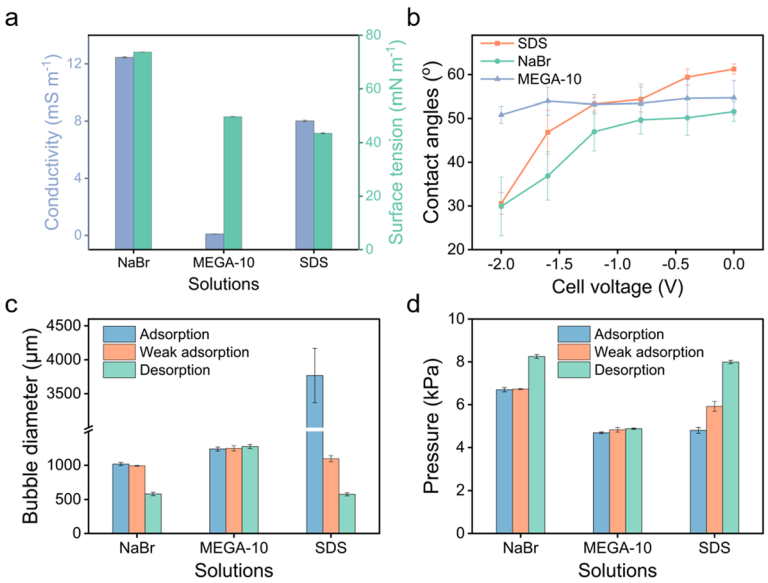

Fig. 5 Tunability of anionic surfactants. (a) Electrical conductivities and surface tensions of 1 mmol L^{-1} NaBr, MEGA-10 and SDS solutions; (b) contact angles of Au/SSS in 1 mmol L^{-1} NaBr, MEGA-10 and SDS aqueous solutions measured by captive bubble method across different electrode potentials with a two-electrode system; (c) bubble diameters and (d) transmembrane pressures for ERLGS with pore size of 33 μm in different states in 1 mmol L^{-1} NaBr, MEGA-10 and SDS aqueous solutions.

4 Experiments

4.1 Materials

Sodium dodecyl sulfate (SDS) was purchased from Shanghai Bide Pharmatech Co., Ltd. Sodium perchlorate monohydrate ($NaClO_4 \cdot H_2O$), potassium nitrate (KNO_3) and ethanol were purchased from Sinopharm Chemical Reagent Co., Ltd. Cysteamine was purchased from Tokyo Chemical Industry Co., Ltd. Sodium Bromide (NaBr) was purchased from Shanghai Titan Scientific Co., Ltd. *N*-Decanoyl-*N*-methylglucamine (MEGA-10) was purchased from Shanghai Aladdin Biochemical Technology Co., Ltd. AISI 304 stainless-steel sheet (SSS) was purchased from Guangzhou Kerong Biological Co., Ltd. All chemicals were used as received. Milli-Q deionized water with a resistivity of 18.2 MΩ cm was used.

4.2 Preparation of ERLGS

The microporous membrane (Au/SSM) was prepared by depositing a 100 nm thick layer of Au on a microporous stainless-steel membrane (SSM) through magnetron sputtering (Discovery 635, Denton vacuum). The stainless-steel membrane was fabricated from SSS by laser drilling with a laser microdrilling machine (YT-XC 300, Yintao Laser Equipment Technology Co., LTD). The size of pore can be controlled by adjusting the laser intensity and spot size. Then ERLGS was obtained by compositing the Au-coated SSM with SDS solution.

4.3 Characterizations

Contact angles (CAs), adsorption kinetics and bubble adhesion force measurements were conducted on an optical surface analyser (LSA 200, LAUDA). CAs were measured by the captive bubble method, which involved the introduction of a small air bubble (5 μL) under a liquid medium against the solid surface. The adsorption kinetics of SDS were obtained by measuring the dynamic surface tensions of the freshly generated pendant bubbles in SDS solutions. And the surface's adhesion force to bubbles were measured by moving the surface to touch the pendant bubbles and then pulling it apart under SDS solution, and calculated by the interface contour. Differential capacitance and open circuit potential of the Au surface in 1 mmol L^{-1} $NaClO_4$ was measured by an impedance/gain-phase analyzer (SI 1260, Solartron Metrology) and an electrochemical workstation (CHI 660 E, CH Instrument Inc.), respectively. The zeta potential of the Au surface in 1 mmol L^{-1} KNO_3 solution was measured by a solid surface charge analyzer (Surpass 3, Anton Paar). To avoid the influence of pore structure, Au-coated stainless-steel sheet (Au/SSS) was used for all above related measurements.

Surface tension measurements of SDS solutions with different concentrations were conducted on a force tensiometer (K100, KRUSS). The electrical conductivities of different solutions were measured by a conductivity meter (TetraCon 325, WTW).

The adsorption of SDS on the Au-coated quartz crystal sensor was measured by a quartz crystal microbalance (QCM 922A, Princeton Applied Research). Deionized water was taken as the base liquid and the baseline frequency signal was measured after it was stable. Then a solution of SDS was added into the cell to make the concentration of SDS is 1 mmol L^{-1}. And the decrease in frequency caused by adsorption were recorded. In order to obtain positively charged surface, the Au-coated quartz crystal was immersed in 1 mmol L^{-1} ethanol solution of cysteamine for 24 h and followed by washing with ethanol and water successively. Then the adsorption behaviour of SDS was measured by the same method as above.

A confocal microprobe Raman system (XploRA, HORIBA, and 638 nm excitation light) and a homemade spectroelectrochemical cell, containing a Pt wire and a saturated calomel electrode (SCE) as the counter and reference electrodes, were used in electrochemical surface-enhanced Raman spectroscopy (EC-SERS) measurements. The Au electrode coated with Au nanoparticles was used as the working electrode and the electrolyte solution employed was 1 mmol L^{-1} SDS aqueous solution. Raman spectroscopy of pure SDS were also measured.

A three-electrode system and a CHI 660 E electrochemical workstation (CH Instrument Inc.) were used in all electrochemical measurements unless otherwise noted. Au surface was served as the working electrode. A saturated calomel electrode (SCE) and a platinum (Pt) wire were used as the reference electrode and the counter electrode, respectively. For the bubble adhesion force and the followed transmembrane pressure measurements, a two-electrode system and a DC power supply (IV 3610, IVYTECH) were used. Au surface and a Pt wire were served as the working electrode and the counter electrode, respectively.

4.4 Controllable microbubble generation

The Au/SSM and SDS aqueous solution (about 3 cm high) were placed in a self-designed setup. The Au/SSM served as the working electrode and the Pt wire was used as the counter electrode. −2.0 V, −0.4 V and 0.0 V were selected as the potentials for desorption, weak adsorption and adsorption states, respectively. When measuring, potential was applied to control the state of system, then air was pressurized through the ERLGS with a constant flow rate of 0.05 mL min^{-1} controlled by a Harvard Apparatus PHD ULTRA syringe pump and microbubbles were generated during the membrane dispersion process. The photographs of the generated bubbles were taken by a digital camera (D750, Nikon) and the sizes of bubbles were obtained. The *in situ* growth processes of bubbles were recorded in a special homemade setup by high-speed videos captured using a i-SPEED 7 camera (iX Cameras) at a frame rate of around 5000 fps. The transmembrane pressure, which is the difference between the gas inlet and outlet of the system, was measured by a laboratory-made pressure sensor.

Data availability statement

The data supporting this article have been included as part of the ESI.†

Conflicts of interest

There are no conflicts to declare.

Acknowledgements

This work was supported by the National Natural Science Foundation of China (52025132, 52300138, 21621091, 22021001, and 22121001), the National Postdoctoral Program for Innovative Talents (BX20230198), the China Postdoctoral Science Foundation (2023M732945), the Higher Education Discipline Innovation Project (B17027, B16029), the Natural Science Foundation of Fujian Province of China (2022J02059, 2023J05012), the Science and Technology Projects of Innovation Laboratory for Sciences and Technologies of Energy Materials of Fujian Province (IKKEM) (RD2022070601), and the New Cornerstone Science Foundation through the XPLORER PRIZE.

References

1 Y. He, T. Zhang, L. Lv, W. Tang, Y. Wang, J. Zhou and S. Tang, Application of microbubbles in chemistry, wastewater treatment, medicine, cosmetics, and agriculture: A review, *Environ. Chem. Lett.*, 2023, **21**, 3245–3271.

2 Y. Zhou, L. Dai and N. Jiao, Review of bubble applications in microrobotics: Propulsion, manipulation, and assembly, *Micromachines*, 2022, **13**, 1068.

3 C. Qiao, D. Yang, X. Mao, L. Xie, L. Gong, X. Peng, Q. Peng, T. Wang, H. Zhang and H. Zeng, Recent advances in bubble-based technologies: Underlying interaction mechanisms and applications, *Appl. Phys. Rev.*, 2021, **8**, 011315.

4 I. Levitsky, D. Tavor and V. Gitis, Micro and nanobubbles in water and wastewater treatment: A state-of-the-art review, *J. Water Process Eng.*, 2022, **47**, 102688.

5 Z. Y. Chang, S. S. Niu, Z. C. Shen, L. C. Zou and H. J. Wang, Latest advances and progress in the microbubble flotation of fine minerals: Microbubble preparation, equipment, and applications, *Int. J. Miner., Metall. Mater.*, 2023, **30**, 1244–1260.

6 X. Li, C. Liu, F. Liu, X. Zhang, X. Chen, Q. Peng, G. Wu and Z. Zhao, Substantial removal of four pesticide residues in three fruits with ozone microbubbles, *Food Chem.*, 2024, **441**, 138293.

7 F. Micaletti, J.-M. Escoffre, S. Kerneis, A. Bouakaz, J. J. Galvin, L. Boullaud and D. Bakhos, Microbubble-assisted ultrasound for inner ear drug delivery, *Adv. Drug Delivery Rev.*, 2024, **204**, 115145.

8 B. Thomas, D. Ohde, S. Matthes, P. Bubenheim, K. Terasaka, M. Schlüter and A. Liese, Enhanced enzyme stability and gas utilization by microbubble aeration applying microporous aerators, *Catal. Sci. Technol.*, 2023, **13**, 1098–1110.

9 M. U. Jung, Y. C. Kim, G. Bournival and S. Ata, Industrial application of microbubble generation methods for recovering fine particles through froth flotation: A review of the state-of-the-art and perspectives, *Adv. Colloid Interface Sci.*, 2023, **322**, 103047.

10 X. Y. Wang, Y. L. Zhu, Y. Shuai, Y. Yang, Z. L. Huang, J. D. Wang and Y. R. Yang, Bubble size "bimodal" distribution enhances mixing and mass transfer in slurry bubbling column reactor, *Ind. Eng. Chem. Res.*, 2024, **63**, 7401–7414.

11 A. S. Reis, T. F. Mendes, I. Petri Júnior and M. A. S. Barrozo, Influence of bubble size on performance of apatite flotation of different particle sizes, *Part. Sci. Technol.*, 2023, **41**, 1044–1052.

12 N. Palya and D. W. MacPhee, Effect of bubble size and column depth on diffused aerator efficiency, *Energy Effic.*, 2023, **16**, 3.

13 Y. Zhang, Y. Han, X. Ji, D. Zang, L. Qiao, Z. Sheng, C. Wang, S. Wang, M. Wang, Y. Hou, X. Chen and X. Hou, Continuous air purification by aqueous interface filtration and absorption, *Nature*, 2022, **610**, 74–80.

14 C. M. Yu, M. Y. Cao, Z. C. Dong, K. Li, C. L. Yu, J. M. Wang and L. Jiang, Aerophilic electrode with cone shape for continuous generation and efficient collection of H_2 bubbles, *Adv. Funct. Mater.*, 2016, **26**, 6830–6835.

15 W. H. Zhang, J. Z. Zhang, B. Zhao and P. H. Zhu, Microbubble size distribution measurement in a DAF system, *Ind. Eng. Chem. Res.*, 2015, **54**, 5179–5183.

16 P. Dijkmans, L. Juffermans, R. Musters, A. Vanwamel, F. Tencate, W. Vangilst, C. Visser, N. Dejong and O. Kamp, Microbubbles and ultrasound: From diagnosis to therapy, *Eur. J. Echocardiogr.*, 2004, **5**, 245–256.

17 Y. Feng, H. Mu, X. Liu, Z. Huang, H. Zhang, J. Wang and Y. Yang, Leveraging 3D printing for the design of high-performance venturi microbubble generators, *Ind. Eng. Chem. Res.*, 2020, **59**, 8447–8455.

18 S. L. Anna, Droplets and bubbles in microfluidic devices, *Annu. Rev. Fluid Mech.*, 2016, **48**, 285–309.

19 B. Q. Xie, C. J. Zhou, L. Sang, X. D. Ma and J. S. Zhang, Preparation and characterization of microbubbles with a porous ceramic membrane, *Chem. Eng. Process.*, 2021, **159**, 108213.

20 J. N. B. Lin, S. K. Banerji and H. Yasuda, Role of interfacial tension in the formation and the detachment of air bubbles. 1. A single hole on a horizontal plane immersed in water, *Langmuir*, 1994, **10**, 936–942.

21 M. Kukizaki and T. Wada, Effect of the membrane wettability on the size and size distribution of microbubbles formed from Shirasu-porous-glass (SPG) membranes, *Colloids Surf., A*, 2008, **317**, 146–154.

22 D. J. Wesley, R. M. Smith, W. B. Zimmerman and J. R. Howse, Influence of surface wettability on microbubble formation, *Langmuir*, 2016, **32**, 1269–1278.

23 S. Khirani, P. Kunwapanitchakul, F. Augier, C. Guigui, P. Guiraud and G. Hébrard, Microbubble generation through porous membrane under aqueous or organic liquid shear flow, *Ind. Eng. Chem. Res.*, 2011, **51**, 1997–2009.

24 B. Q. Xie, C. J. Zhou, X. T. Huang, J. X. Chen, X. D. Ma and J. S. Zhang, Microbubble generation in organic solvents by

porous membranes with different membrane wettabilities, *Ind. Eng. Chem. Res.*, 2021, **60**, 8579–8587.
25 X. Hou, Y. Hu, A. Grinthal, M. Khan and J. Aizenberg, Liquid-based gating mechanism with tunable multiphase selectivity and antifouling behaviour, *Nature*, 2015, **519**, 70–73.
26 J. Zhang, B. Y. Chen, X. Y. Chen and X. Hou, Liquid-based adaptive structural materials, *Adv. Mater.*, 2021, **33**, 2005664.
27 S. Yu, L. Pan, Y. Zhang, X. Chen and X. Hou, Liquid gating technology, *Pure Appl. Chem.*, 2021, **93**, 1353–1370.
28 S. Wang, Y. Zhang, Y. Han, Y. Hou, Y. Fan and X. Hou, Design of porous membranes by liquid gating technology, *Acc. Mater. Res.*, 2021, **2**, 407–419.
29 R. R. Zhang, J. M. Lei, J. D. Xu, H. X. Fu, Y. Jing, B. Y. Chen and X. Hou, Bioinspired photo-responsive liquid gating membrane, *Biomimetics*, 2022, **7**, 47.
30 B. Y. Chen, R. R. Zhang, Y. Q. Hou, J. Zhang, S. Y. Chen, Y. H. Han, X. Y. Chen and X. Hou, Light-responsive and corrosion-resistant gas valve with non-thermal effective liquid-gating positional flow control, *Light: Sci. Appl.*, 2021, **10**, 127.
31 J. Liu, X. Xu, Y. Lei, M. Zhang, Z. Sheng, H. Wang, M. Cao, J. Zhang and X. Hou, Liquid Gating Meniscus-shaped deformable magnetoelastic membranes with self-driven regulation of gas/liquid release, *Adv. Mater.*, 2021, **34**, e2107327.
32 Z. Z. Sheng, M. C. Zhang, J. Liu, P. Malgaretti, J. Y. Li, S. L. Wang, W. Lv, R. R. Zhang, Y. Fan, Y. M. Zhang, X. Y. Chen and X. Hou, Reconfiguring confined magnetic colloids with tunable fluid transport behavior, *Natl. Sci. Rev.*, 2021, **8**, nwaa301.
33 B. Chen, M. Zhang, Y. Hou, H. Wang, R. Zhang, Y. Fan, X. Chen and X. Hou, Energy saving thermal adaptive liquid gating system, *Innovation*, 2022, **3**, 100231.
34 J. Liu, Z. Sheng, M. Zhang, J. Li, Y. Zhang, X. Xu, S. Yu, M. Cao and X. Hou, Non-Newtonian fluid gating membranes with acoustically responsive and self-protective gas transport control, *Mater. Horiz.*, 2023, **10**, 899–907.
35 Z. Z. Sheng, H. L. Wang, Y. L. Tang, M. Wang, L. Z. Huang, L. L. Min, H. Q. Meng, S. Y. Chen, L. Jiang and X. Hou, Liquid gating elastomeric porous system with dynamically controllable gas/liquid transport, *Sci. Adv.*, 2018, **4**, eaao6724.
36 W. Lv, Z. Sheng, Y. Zhu, J. Liu, Y. Lei, R. Zhang, X. Chen and X. Hou, Highly stretchable and reliable graphene oxide-reinforced liquid gating membranes for tunable gas/liquid transport, *Microsyst. Nanoeng.*, 2020, **6**, 43.
37 Y. Fan, Z. Z. Sheng, J. Chen, H. Pan, B. Y. Chen, F. Wu, S. L. Wang, X. Y. Chen and X. Hou, Visual chemical detection mechanism by a liquid gating system with dipole-induced interfacial molecular reconfiguration, *Angew. Chem., Int. Ed.*, 2019, **58**, 3967–3971.
38 H. M. Wang, Y. Fan, Y. Q. Hou, B. Y. Chen, J. M. Lei, S. J. Yu, X. Y. Chen and X. Hou, Host-guest liquid gating mechanism with specific recognition interface behavior for universal quantitative chemical detection, *Nat. Commun.*, 2022, **13**, 1906.
39 S. J. Yu, Y. Jing, Y. Fan, L. H. Xiong, H. M. Wang, J. M. Lei, Y. M. Zhang, J. Liu, S. L. Wang, X. Y. Chen, H. Sun and X. Hou, Ultrahigh efficient emulsification with drag-reducing liquid gating interfacial behavior br, *Proc. Natl. Acad. Sci. U. S. A.*, 2022, **119**, e2206462119.
40 D. Yu, X. Xiao, C. Shokoohi, Y. Wang, L. Sun, Z. Juan, M. J. Kipper, J. Tang, L. Huang, G. S. Han, H. S. Jung and J. Chen, Recent advances in stimuli-responsive smart membranes for nanofiltration, *Adv. Funct. Mater.*, 2022, **33**, 2211983.
41 S. Ogata, K. Shigehara, T. Yoshida and H. Shinohara, Small bubble formation by using strong nonuniform electric field, *IEEE Trans. Ind. Appl.*, 1980, **IA-16**, 766–770.
42 C. Tsouris, W.-T. Shin, S. Yiacoumi and D. W. DePaoli, Electrohydrodynamic velocity and pumping measurements in water and alcohols, *J. Colloid Interface Sci.*, 2000, **229**, 335–345.
43 P. Di Marco, W. Grassi, G. Memoli, T. Takamasa, A. Tomiyama and S. Hosokawa, Influence of electric field on single gas-bubble growth and detachment in microgravity, *Int. J. Multiphase Flow*, 2003, **29**, 559–578.
44 W. Zhang, J. Wang, Q. Su, B. Li, K. Yu, H. Xu, L. Zuo and T. Wu, Polarization motion of bubbles in a non-uniform electric field, *Chem. Eng. J.*, 2023, **455**, 140767.
45 M. H. Chen, I. Burgess and J. Lipkowski, Potential controlled surface aggregation of surfactants at electrode surfaces - A molecular view, *Surf. Sci.*, 2009, **603**, 1878–1891.
46 M. Jaschke, H. J. Butt, H. E. Gaub and S. Manne, Surfactant aggregates at a metal surface, *Langmuir*, 1997, **13**, 1381–1384.
47 Y. Liu, N. Peng, Y. F. Yao, X. Zhang, X. Q. Peng, L. Y. Zhao, J. Wang, L. Peng, Z. K. Wang, K. Mochizuki, M. Yue and S. K. Yang, Breaking the nanoparticle's dispersible limit via rotatable surface ligands, *Nat. Commun.*, 2022, **13**, 3581.
48 J. J. Leitch, J. Collins, A. K. Friedrich, U. Stimming, J. R. Dutcher and J. Lipkowski, Infrared studies of the potential controlled adsorption of sodium dodecyl sulfate at the Au(111) electrode surface, *Langmuir*, 2012, **28**, 2455–2464.
49 R. J. Pugh, *Bubble and foam chemistry*, Cambridge University Press, Cambridge, 2016.
50 A. A. Papaderakis and R. A. W. Dryfe, The renaissance of electrowetting, *Curr. Opin. Electrochem.*, 2023, **38**, 101245.
51 M. Mietton-Peuchot, Use of gas-liquid porometry measurements for selection of microfiltration membranes, *J. Membr. Sci.*, 1997, **133**, 73–82.
52 M. J. Rosen and J. T. Kunjappu, *Surfactants and interfacial phenomena*, John Wiley & Sons, New Jersey, 2012.